International Journal of Nanomedicine

Dovepress

open access to scientific and medical research

Open Access Full Text Article

ORIGINAL RESEARCH

A Yeast Cell Wall Derived Hybrid Hydrogel with Photothermal and Immune Combined Modality Therapy for Enhanced Anti-Melanoma Efficacy

Chen Yang[1], Jiaxing Lei[1], Ximeng Kang[1], Peipei Zhang[1], Shaohua Zheng[2], Qingqing Li[1], Jiye Zhang[1]

[1]School of Pharmacy, Health Science Center, Xi'an Jiaotong University, Xi'an, People's Republic of China; [2]The First Affiliated Hospital of Xi'an Jiaotong University, Xi'an, People's Republic of China

Correspondence: Qingqing Li; Jiye Zhang, School of Pharmacy, Health Science Center, Xi'an Jiaotong University, No. 76 Yanta Westroad, Xi'an, People's Republic of China, Email liqingqing0217@mail.xjtu.edu.cn; zjy2011@mail.xjtu.edu.cn

Introduction: The effect of traditional treatment for melanoma is quite limited, especially for its recurrence. As the major components of yeast cell wall, chitin and β-glucan exhibit good immune activation effect and are promising candidates for adjuvant. Therefore, melanoma cell membrane (CM) and indocyanine green (ICG) was loaded in a chitin and β-glucan hybrid hydrogel to achieve an enhanced anti-melanoma therapy.

Methods: The novel hybrid hydrogel was prepared, and its physicochemical properties were examined. Its effect towards melanoma prevention and treatment was evaluated via a melanoma-bearing mice model.

Results: The CM-ICG-hybrid hydrogel was successfully prepared with excellent injectability, self-healing, drug loading, rheological, in vitro and in vivo photothermal stability, and retention properties. It also exhibited good cellular and in vivo safety profiles. In the primary melanoma mice model, it quickly ablated the in-situ melanoma, effectively inhibited the tumor growth, increased the survival rate of melanoma-bearing mice, and increased the level of IFN-γ and TNF-α. In the distal secondary melanoma model, it efficiently prevented the reoccurrence of melanoma and activated the memory T cells. In both models, a synergistic effect of photothermal therapy and immune therapy was found. The hydrogel effectively recruited $CD3^+$ $CD4^+$ T cells and $CD3^+$ $CD8^+$ T cells, inhibited the proliferation of melanoma cells, and induced the apoptosis of melanoma cells.

Conclusion: The hybrid hydrogel was successfully prepared, and it showed excellent efficacy towards melanoma prevention and treatment due to its efficient tumor ablation and immune activation capability.

Keywords: chitin, β-glucan, hybrid hydrogel, melanoma cell membrane, photo thermotherapy, immunotherapy

Introduction

Melanoma, generally referred to as malignant melanoma, is derived from the malignant transformation of nerves and melanocytes in skin.[1] It is the most aggressive skin cancer.[1,2] Except for the difficulty in diagnosis, melanoma also has high risk of metastasis and recurrence, poor prognosis, and low five-year survival rate.[2,3] At present, surgical resection is still the most popular treatment for melanoma.[4,5] However, due to its limited surgery scope, its effects for advanced melanoma and melanoma with lymph node metastasis are poor.[4,6,7] Chemotherapy is commonly accompanied with strong side effects and high risk of tumor resistance and tumor metastasis.[3–5] Radiation therapy also elicits strong side effects, immunosuppression, and tumor metastasis.[1,4,8,9]

Photothermal therapy (PTT) can rapidly ablate most in-situ tumors due to the high targeting effect, small wound surface, and low side effects. Shao et al reported that a black phosphorus quantum dots-PLGA nanosphere-based PTT showed good biocompatibility as well as excellent PTT efficiency and breast tumor ablation effect. There was no recurrence during the observation period.[10] Heidari et al used indocyanine green (ICG) and gold-ferrite nanocomposite as photothermal agents, and the tumors of mice could also be ablated after PTT.[11] Indocyanine green is an FDA-approved near-infrared dye.[12–14] It is also a photosensitizer with high photothermal conversion efficiency.[12] When the temperature of the tumor exceeds 45°C, protein

Received: 10 March 2023
Accepted: 28 August 2023
Published: 21 September 2023

Graphical Abstract

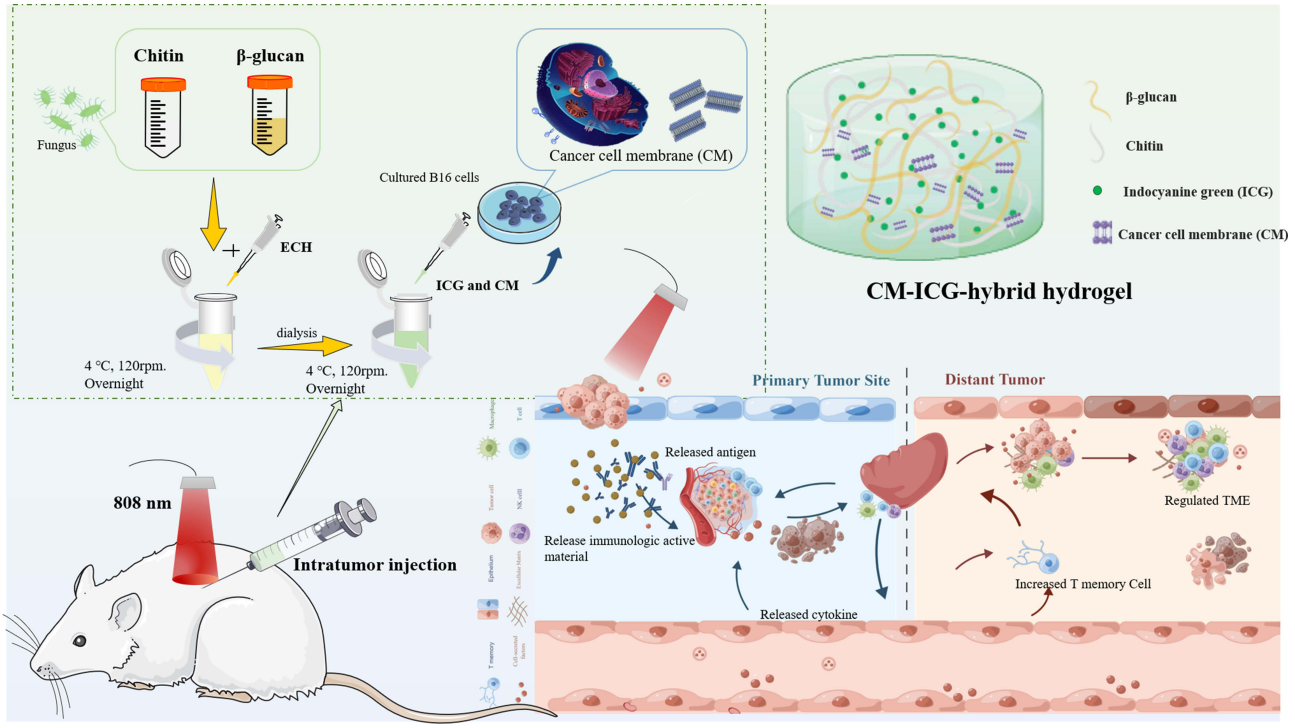

starts to denature and the cell membrane begins to rupture, which leads to immunogenic cell death.[13–15] However, photothermal therapy is not effective for advanced complex diffuse tumors, metastases, and recurrent tumors.[13,15–17]

Immunotherapy is a novel potential method of tumor treatment.[18,19] A large number of monoclonal antibodies based on immune checkpoint inhibitors have been approved and launched on the market. For example, the approved anti-PD-1 antibodies nebuliumab and pabolizumab are effective in patients with BRAF mutations and BRAF inhibitor refractory diseases.[20] Talimogene laherparepvec (T-VEC) replicates within tumor cells and produces granulocyte-macrophage colony-stimulating factor. Intratumor injection of T-VEC could result in tumor cell lysis and continuous release of tumor-specific antigens. Patients treated with T-VEC had a significant 16.3% improvement in the rate of durable response. A recently published phase Ib trial using ipilimumab and T-VEC showed a tolerable safety profile with an overall response rate of 50%.[21] Immunotherapy activates the body's immune system to fight tumor cells.[22] In a certain period of time after immunotherapy, the tumor in the body is still suppressed by the immune system, which reduces tumor metastasis and recurrence.[7,23] For some advanced patients who are unable to be treated by surgery or chemotherapy, and for patients with lymph node metastasis, immunotherapy shows promising therapeutic effect.[7,23]

For melanoma patients, the immune responses are generally at low levels due to immunosuppression and tumor heterogeneity, which attenuates the effect of immunotherapy.[24–27] In addition, due to scarce known tumor antigens and ambiguous mechanisms, developing a highly effective tumor vaccine for a specific tumor is quite challenging. The tumor cell membrane locates on the surface of the tumor and is a subcellular source of tumor, which consists of nearly all the antigens of the tumor cell, which can effectively improve the specific antitumor responses and inhibit tumor recurrence by activating durable immune memory effects.[28–30] However, tumor-associated antigens alone cannot elicit sufficient tumor-suppressive immune responses.[28–30] Although the supplement of tumor-associated antigens can promote the recognition and localization of tumor tissue, the lack of tumor costimulatory factors makes T cells unable to play their role and generally collapse. Thus, immunostimulatory adjuvants are generally added in practical application to enhance

the immune recognition and stimulation.[24,28–31] In particular, immune adjuvants that can activate antigen-presenting cells play a key role in anti-tumor activity via facilitating the uptake and presentation of antigens to T cells.

Chitin and β-glucan are the main components of fungal cell walls,[32,33] which have strong immunogenicity. Chitin can stimulate the production of macrophages and activate non-specific immune response after being recognized and degraded by chitinase in vivo.[34,35] β-Glucan can be specifically recognized, captured, and degraded into fragments by macrophages in vivo.[33,36–38] These fragments bind to neutrophils, natural killer cells, and lymphocytes; activate dendritic cells, neutrophils, NK cells, and PI3K signaling pathways; they thereby stimulate humoral and cellular immunity, resulting in tumor cell ablation.[32,37,38] In our previous studies, a novel injectable hybrid hydrogel composed of chitin and β-glucan was synthesized that could effectively adjust the immune responses in the Balb/c mice.[32]

In this study, the chitin and β-glucan hybrid hydrogel acts not only as an immunostimulatory adjuvant but also as a delivery system which delivers ICG and melanoma cell membrane directly into the tumor via intratumor injection. Our hypothesis is that the CM-ICG-hybrid hydrogel could effectively ablate and prevent the melanoma due to the combination of photothermal therapy and immunotherapy. We aimed to: (1) fabricate and physically characterize CM-ICG-hybrid hydrogel; (2) evaluate the in-situ anti-melanoma effect of the hydrogel in a mice melanoma model; and (3) evaluate the melanoma-preventing effect of the hydrogel in a distal melanoma model in mice. Our research represented the first systematic study of applying chitin and β-glucan hybrid hydrogel as both immunostimulatory adjuvant and delivery system to achieve the combination of photothermal therapy and immunotherapy. It laid the groundwork for clinical translation.

Experimental

Materials

Chitin was purchased from Golden Shell Co., Ltd (Zhejiang, China), and β-glucan was obtained from Tianxiangyuan Co., Ltd (Zhuhai, China). Indocyanine Green (ICG) was obtained from BBI Life Sciences Co., Ltd (Shanghai, China). Epichlorohydrin was bought from Energy Chemical (Anhui, China). Carbamide was purchased from Macklin (Shanghai, China). The ki-67 detection kit, TUNEL detection kit, and the Hematoxylin and Eosin Staining Kit were purchased from Servicebio (Wuhan, China). ELISA kits for TNF-α and IFN-γ were purchased from Elabscience (Wuhan, China). The Calcein AM/PI staining kit was obtained from GuYoo (Nanjing, China). The Cell Counting Kit (CCK-8) was bought from GLPBIO (US). Antibodies against cell surface markers for flow cytometry assay were purchased from Biolegend (US).

Cell Culture

The B16F10 cells were bought from Cell Bank, Chinese Academy of Sciences (Shanghai), and were cultured in DMEM medium with 10% FBS at 37°C with 5% CO_2.

Methods

B16F10 Cell Membrane Harvest

B16F10 cells were cultured in a DMEM medium with 10% FBS at 37°C with 5% CO_2. The cell membranes of B16F10 cells (CM) were harvested based on a method reported earlier with modification.[39,40] Briefly, B16F10 cells were collected when after 80% confluence. The cells were subsequently resuspended in Tris-HCl buffer with 1% phenylmethanesulfonyl fluoride and were lysed by an ultrasonic cell disruptor (SIENTZ, China). Afterwards, the cell lysate was centrifuged at 3000 *g*, 4°C for 10 min. The obtained supernatant was centrifuged again at 20,000 *g* via an ultra-high-speed refrigerated centrifuge (Hitachi, Japan, Tokyo) for 20 min. The precipitate was collected, washed with deionized water, then stored at −80°C for later use.

The Quantification and Characterization of the Protein in CM

The total protein content in CM was quantified by a protein quantification kit. The proteins of CM were characterized by sodium dodecyl sulfate-polyacrylamide gel electrophoresis.

Preparation of a Hybrid Hydrogel Composed of β-Glucan and Chitin

The hybrid hydrogel was prepared via a chemical cross-linking method.[41] Briefly, 1.5 g of chitin powder or 6 g of β-glucan powder was added in 100 mL of NaOH (8%)-urea (4%) aqueous solution and was frozen at −30°C for 4 hours before being thawed at room temperature. This freeze-thaw cycle was repeated for 3 times until the chitin or β-glucan was completely dissolved. Next, 0.8 mL of the chitin solution and 0.2 mL of the β-glucan were withdrawn and mixed with 20 μL of epichlorohydrin and shaken (200 rpm) for 8 hours until a hybrid hydrogel was obtained. Finally, the hybrid hydrogel was dialyzed in a normal saline solution at 37°C to remove the NaOH and urea in the hydrogel. The β-glucan hydrogel and chitin hydrogel were prepared in a similar way.

Preparation of CM and Indocyanine Green Co-Loaded Hybrid Hydrogel

Fifty μL of indocyanine green (ICG) aqueous solution (50 mg/mL) and 100 μL of CM suspension (protein concentration was 166.7 μg/mL) were mixed before being added into 1 mL of the hybrid hydrogel, which was subsequently shaken (4°C, 200 rpm) in the dark for 8 h until a uniformly colored CM-ICG-hybrid hydrogel was obtained. CM-ICG-Chitin hydrogel and CM-ICG-β-glucan hydrogel were prepared with a similar method.

Surface Morphology of the CM-ICG-Hybrid Hydrogel

The surface morphology of the CM-ICG-hybrid hydrogel was captured by a scanning electron microscope (Higuchi, Japan) after being freeze-dried and sputtered with gold.

Rheological Properties of the CM-ICG-Hybrid Hydrogel

The rheological properties of the CM-ICG-hybrid hydrogel were examined via an advanced rotational rheometer (ANTON PAAR GMBH, Graz, Austria). A time versus storage modulus (G') and loss modulus (G") curve was drawn to record the rheology.

Cytotoxicity of the CM-ICG-Hybrid Hydrogel With or Without Laser

The cytotoxicity of the CM-ICG-hybrid hydrogel on B16F10 cells with or without an 808 nm near-infrared laser irradiation was detected via a CCK-8 kit and a Calcein-AM/PI kit according to the manufacturers' instructions. For detailed procedures, please refer to Section S1 and S2.

In vitro Photothermal Effect of the CM-ICG-Hybrid Hydrogel

A quantity of 1 mL of CM-ICG-hybrid hydrogel was placed in an Ep tube before being irradiated with an 808 nm laser (Viasho, China, Beijing) for 5 minutes. The temperature of the hydrogel was monitored with a FLIR C2 infrared image camera (FLIR systems, Inc., USA). A temperature versus irradiation time curve was drawn to record the in vitro photothermal effect of the hydrogel.

In vitro Photothermal Stability of the CM-ICG-Hybrid Hydrogel

A total of 1 mL of the CM-ICG-hybrid hydrogel was placed in an Ep tube before being irradiated with laser for 5 minutes. After the hydrogel was cooled to room temperature, it was re-irradiated with laser for another 5 minutes. This laser irradiation–cool down process was repeated 5 times, and the temperature change of the hydrogel was monitored with a FLIR C2 infrared imaging camera. A temperature versus irradiation time curve was plotted to evaluate the in vitro photothermal stability of the hydrogel.

Animals

C57BL/6J mice (female, 6 to 8 weeks) were purchased from the Laboratory Animal Service Center of Xi'an Jiaotong University. All animal experiment procedures adhered strictly to the *Laboratory Animal-Guideline for ethical review of animal welfare* and were approved by the Institutional Animal Ethical Committee of the Xi'an Jiaotong University, and the approval number is SCXK (Shaanxi) 2021–103.

In vivo Photothermal Effect of the CM-ICG-Hybrid Hydrogel

Six healthy C57BL/6J mice were anesthetized via being placed in a RWD R550 multi-channel small animal anesthesia machine (RWD, China) with isoflurane. A total of 100 μL of CM-ICG-hybrid hydrogel was subcutaneously injected.

Next, the injection site of the mice was irradiated with laser for 5 minutes and the temperature was monitored with a FLIR C2 infrared imaging camera. A temperature versus irradiation time curve was plotted to evaluate the in vivo photothermal effect of the hydrogel.

In vivo Retention Time of the CM-ICG-Hybrid Hydrogel

Twelve healthy C57BL/6J mice were anesthetized with isoflurane and randomly divided into two groups (6 mice/group). A total 100 μL of CM-ICG-hybrid hydrogel or free ICG was subcutaneously injected, respectively. An 808 nm near-infrared laser was applied on the injection site on the 1st, 2nd, and 4th day of injection for 5 minutes, respectively. The temperature change of the laser site was recorded by a FLIR C2 infrared imaging camera to evaluate the retention time of the hydrogel in mice.

In vivo Safety of the CM-ICG-Hybrid Hydrogel

Eighteen C57BL/6J mice were anesthetized with isoflurane and were randomly divided into 3 groups, namely control, CM-ICG-hybrid hydrogel (+), and CM-ICG-hybrid hydrogel (-); + denotes with laser illumination, - denotes without laser illumination. A total of 100 μL of CM-ICG-hybrid hydrogel or normal saline was injected subcutaneously into the dorsal depilation area of the mice. For the mice in the CM-ICG-hybrid hydrogel (+) group, an irradiation of an 808 nm laser was applied for 5 minutes. Thirty days later, the hearts, livers, spleens, lungs, and kidneys were collected. The organs were sectioned with an RM2016 pathological microtome. After H+E staining, the images were captured and the pathological changes in each organ were analyzed.

Anti-Primary Melanoma Effect of the CM-ICG-Hybrid Hydrogel

Melanoma Growth Monitor

Ninety C57BL/6J mice were anesthetized with isoflurane before the hair on the dorsal skin was removed by a razor. Next, 100 μL of B16F10 melanoma cell suspension (8×10^5 cells/mL) was subcutaneously injected into the right axilla. The dimension of the tumor was measured with a vernier caliper every 2 to 3 days, and tumor size was calculated according to the following formula: Tumor volume = 1/2 × length × width^2. When the tumor size reached 80 to 100 mm^3, the mice were randomly divided into 9 groups (10 mice/group), namely blank hybrid hydrogel, ICG-hybrid hydrogel (+), CM-hybrid hydrogel, CM-ICG-hybrid hydrogel (-), CM-ICG-hybrid hydrogel (+), CM-ICG-Chitin hydrogel (+), CM-ICG-β-glucan hydrogel (+), CM-ICG-carbomer hydrogel (+), and control. A quantity of 100 μL of normal saline or specific drug delivery system was injected into the melanoma accordingly. Next, the tumor of mice in different groups was irradiated with or without laser for 5 min on the first and third day of the injection. The tumor size of the mice was measured with a vernier caliper every 2 to 3 days, and the survival status of the mice was recorded. Mice were considered dead when the tumor volume exceeded 1000 mm^3. The procedures for CM-ICG-carbomer hydrogel preparation are described in S3 in the Supplementary Materials.

Pathological Analysis of the Melanoma

Seven days after the hydrogel injection, tumors were surgically collected. After being fixed, dehydrated, and embedded in the paraffin, the tumors were sectioned. The image was captured after H+E staining, and pathological changes in tumor were analyzed.

Melanoma Cell Proliferation and Apoptosis Analysis

The effect of CM-ICG-hybrid hydrogel on melanoma cell proliferation was analyzed by a ki-67 immunohistochemistry detection kit, and its effect on melanoma cell apoptosis was analyzed by a TUNEL immunohistochemistry detection kit. The detailed procedures are described in S4 and S5. The quantifications of cells were conducted by Image J.

Immune Activation Effect

The peripheral blood was collected into a sterile anticoagulant tube 7 days after the hydrogel injection. An ELISA kit was used to detect IFN-γ and TNF-α in the blood based on the manufacturer's instructions. The proportion of T cells in the spleen was analyzed via flow cytometry, and the detailed procedures are described in S6 and S7.

Melanoma-Preventing Effect of the CM-ICG-Hybrid Hydrogel

Distal Melanoma Growth Monitor

Eighty C57BL/6J mice were anesthetized with isoflurane before the hair on the dorsal skin was removed by a razor. Next, 100 μL of B16F10 melanoma cell suspension (8×10^5/mL) was subcutaneously injected into the right axilla. The dimension of the tumor was measured with a vernier caliper every 2 to 3 days. When it reached 80 to 100 mm^3, the mice were randomly divided into 8 groups (10 mice/group), and 100 μL of different delivery systems was injected into the melanoma. The primary tumor was removed either by surgical section or photothermal ablation. Three days later, another 100 μL of B16F10 melanoma cell suspension (5×10^5 cells/mL) was subcutaneously injected into the left axilla. The occurrence and size of the second tumor were observed and measured to evaluate the effect of the hydrogel on distal secondary tumors.

T Cell Infiltration in Distal Tumors

The mice were sacrificed by cervical dislocation 21 days after the second tumor inoculation, and the distal tumors were collected. The T cell infiltration in distal tumors was evaluated via flow cytometry analysis and immunofluorescence staining. The specific procedures are described in S8.

Memory T Cell Analysis

The mice were sacrificed by cervical dislocation 21 days after the second tumor inoculation, the spleens were collected, and the proportion of memory T cells was analyzed flow cytometry. The specific procedures are described in S7, S9.

Statistical Analysis

All experiments were conducted in at least triplicate, and results are expressed as mean ± standard deviation. One-way ANOVA with Tukey–Kramer post-hoc test was used to compare differences among three or more groups. $P<0.05$ was considered to be statistically significant.

Results

Preparation and Characterization of CM-ICG-Hybrid Hydrogel

B16F10 cell is a mouse melanoma cell line, and its membrane contains all the surface antigens of the melanoma.[42,43] Gp100 is one of the main components of the melanoma-associated antigens, which can be specifically recognized by the body and activates the immune responses.[42,43] TRP2 is a tyrosinase-associated protease, and it is also a key enzyme in melanin synthesis.[42,44] As shown in Figure 1A, clear Gp100 and TRP2 bands could be observed, which indicated the successful collection of melanoma cell membranes.

The morphology of the chitin and/or β-glucan hydrogels is shown in Figure 1B. Interconnected structures were observed in all hydrogels, the typical micromorphology of hydrogels.[32] Among them, chitin hydrogel exhibited the largest pore size, whereas β-glucan hydrogel exhibited the smallest pore size. The smaller the pore size, the larger the crosslinking density.[45] When the hydrogel with smaller pore size expands, the binding force of the elastic network increases, and its capability of water absorption and dehydration decreases, which results in a smaller elasticity.[45,46] Therefore, the elasticity of chitin hydrogel was the strongest, and the elasticity of β-glucan hydrogel was the smallest. An image of CM-ICG-hybrid hydrogel is shown in Figure 1C; the contents did not flow when the vial was inverted, implying that the hydrogel remained in a good gelation state after CM and ICG were encapsulated.

Next, the rheological properties of the hydrogels were examined. The storage modulus (G') refers to the energy stored during the elastic deformation of a material.[46] The loss modulus (G") reflects the amount of lost energy when the hydrogel recovers from deformation.[47] G' of the three hydrogels were higher than G", which indicated that a stable crosslinking network was formed in the hydrogel.[45,48] Hybrid hydrogel exhibited moderate flexibility and rigidity, which could resist a certain amount of stress. As shown in Figure 1D, there was no significant difference in G' and G" between blank hybrid hydrogel and CM-ICG-hybrid hydrogel, which implied that the addition of CM and ICG did not affect the rheological properties of the hydrogel.

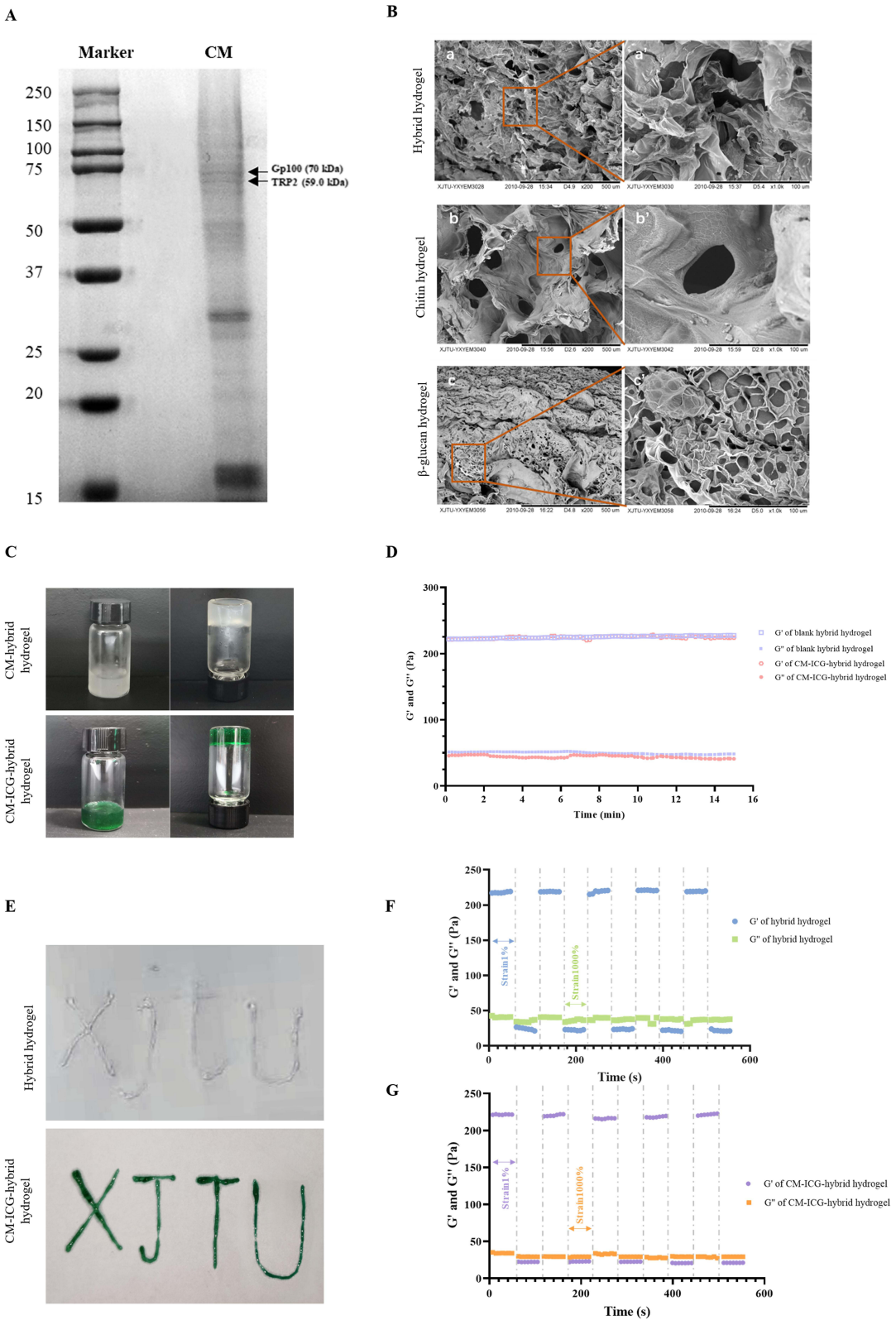

Figure 1 The preparation and characterization of the hybrid hydrogels. (**A**) SDS-PAGE of the protein in the cell membrane of B16F10 cells; (**B**) the SEM images of (a) β-glucan hydrogel, (b) chitin hydrogel, and (c) hybrid hydrogel; (**C**) images of the CM-hybrid hydrogel and ICG-CM-hybrid hydrogel; (**D**) rheological properties of blank hybrid hydrogel and ICG-CM-hybrid hydrogel; (**E**) the injectability of blank hybrid hydrogel and ICG-CM-hybrid hydrogel; (**F**) the self-healing performance of blank hybrid hydrogel; (**G**) the self-healing performance of ICG-CM-hybrid hydrogel.

https://doi.org/10.2147/IJN.S409674 DovePress

The injectability is the key property to achieve in-situ treatment. As shown in Figure 1E, both the blank hybrid hydrogel and CM-ICG-hybrid hydrogel could continuously pass through a 26 G needle and maintained a gelation state after injection, which proved the excellent injectability of the hydrogels. The self-healing properties of the hybrid hydrogel and CM-ICG-hybrid hydrogel are shown in Figure 1F and G. Under high stress (100%), the G' and G' of both hydrogels decreased sharply, recovering quickly under low stress (1%), which indicates the good self-healing capability of the two hybrid hydrogels,[49] allowing the hydrogel to pass through the syringe needle and maintain its original form; this is of great significance for in-situ treatment of tumor.

Photothermal Properties of CM-ICG-Hybrid Hydrogel

The in vitro photothermal properties of CM-ICG-hybrid hydrogel are shown in Figure 2A and B, Figure S1. When a near-infrared laser was applied, the temperature of free ICG solution, ICG-hybrid hydrogel, and CM-ICG-hybrid hydrogel rapidly rose to 60°C within 5 minutes, which indicated that the hybrid hydrogel did not block or impair the photothermal performance of ICG when it was encapsulated in the hybrid. The in vivo photothermal effect is shown in Figure 2C and D; under laser irradiation, the temperature of the skin surrounding the injection site of CM-ICG-hybrid hydrogel increased to above 40°C within 2 minutes and above 50°C within 4 minutes. Various studies reported that when the temperature of the tumor reached above 40°C, immunogenic cell death occurred and released a large number of tumor-associated antigens and damage-related model molecule patterns,[50] which resulted in an elevated immune response in tumor.[50,51] When the temperature is higher than 50°C, heat ablation of tumor would happen.[51] The photothermal stability of the CM-ICG-hybrid hydrogel is shown in Figure 2E; after five consecutive cycles of "laser on–laser off", it still rapidly increased by 30°C within five minutes of laser irradiation. Therefore, the hydrogel exhibited excellent photothermal conversion performance and photothermal stability.

Next, the in vivo photothermal conversion efficiency of CM-ICG-hybrid hydrogel was investigated. As shown in Figure 2F, after 5 minutes of laser treatment, the skin temperature near the injection site of CM-ICG-hybrid hydrogel quickly increased to 50°C for consecutive four days. In contrast, for the free ICG solution group, the skin temperature near the injection site could only reach to 41.2°C on the second day and 33.4°C on the fourth day. Besides, the skin temperature around the injection site of the free ICG solution was high. This implied that the free ICG was not retained in the injection site, which greatly impaired the PTT effect.

Next, a CCK-8 method and Calcein-AM/PI staining were used to clarify the photothermal cell killing effect of CM-ICG-hybrid hydrogel. As shown in Figure 2G and H, the cell viability was lower than 10% for ICG-containing groups with laser irradiation and above 95% for groups without laser irradiation or ICG. Therefore, ICG itself is not cytotoxic, and the cell death was due to the photothermal effect of ICG under laser excitation.

In vivo Safety of CM-ICG-Hybrid Hydrogel

The toxicity CM-ICG-hybrid hydrogel to the main organs was examined after it was subcutaneously injected into the back skin of mice with or without laser (3 times). As shown in Figure S2, no matter whether laser was applied or not, no significant pathological injury was found in the organ sections of the CM-ICG-hybrid hydrogel group, which was also not significantly different from those of healthy mice. This result indicated the good histocompatibility of CM-ICG-hybrid hydrogel.

Anti-Primary Melanoma Effect of the CM-ICG-Hybrid Hydrogel

Melanoma Size Monitor

The anti-primary melanoma effect of the CM-ICG-hybrid hydrogel was evaluated in a melanoma model in C57BL/6J mice, and the specific process is shown in Figure 3A. The body weight of the mice with different treatment is shown in Figure 3B. PTT could effectively ablate the tumor, and the tumor size decreased significantly right after PTT (Figure 3C and D). The size of the tumors in the blank hydrogel group was significantly smaller than that of the control group, which may be due to the innative immunogenicity of chitin and β-glucan.[34,38,52] Compared with the blank hydrogel group, the tumors in the CM-hybrid hydrogel group were significantly smaller, which may be related to the tumor-specific immune response caused by abundant tumor-associated antigen on the CM.[39,40] Compared with the CM-hybrid hydrogel group, the tumor of the CM-

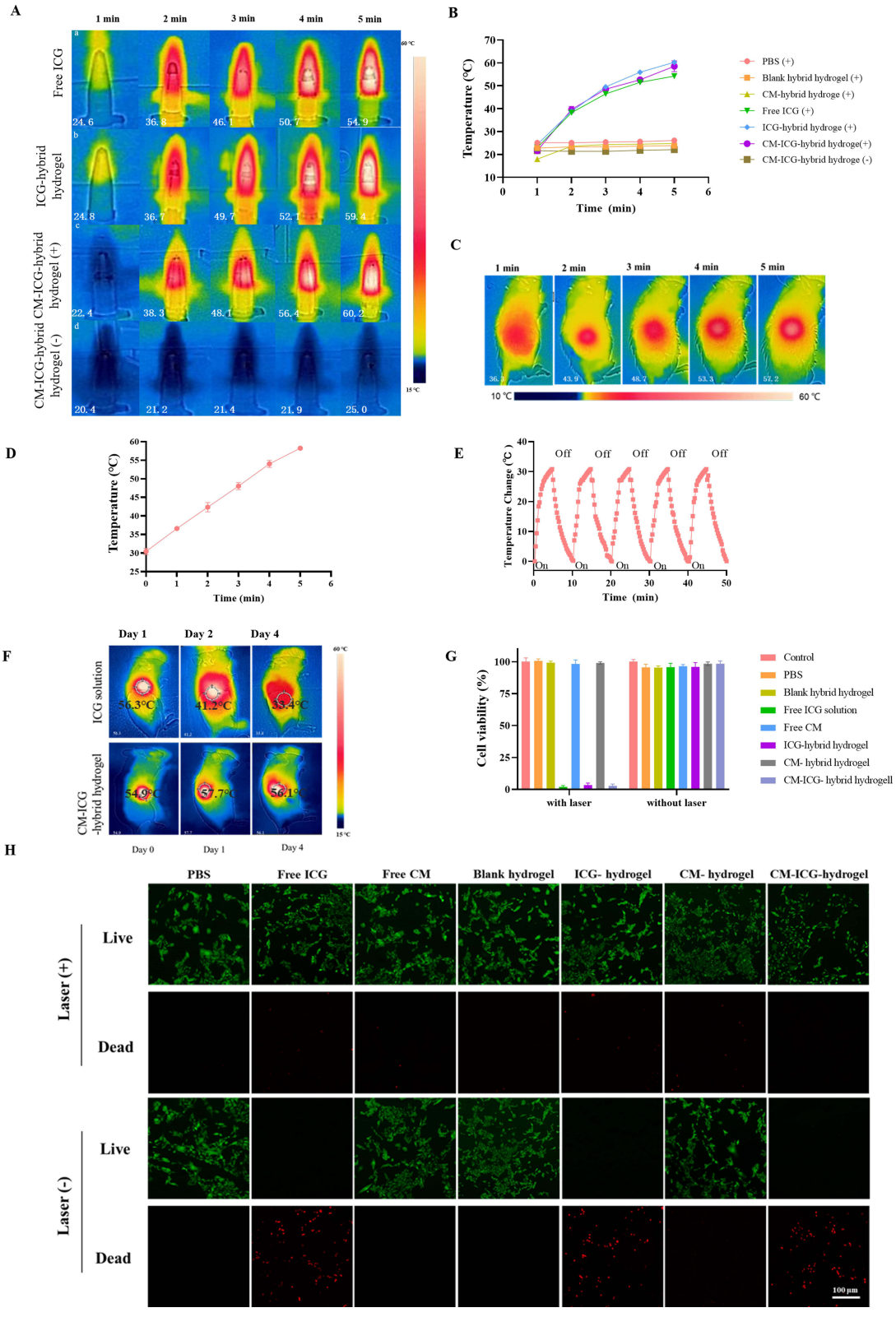

Figure 2 The photothermal properties of the CM-ICG-hybrid hydrogels. (**A** and **B**) In vitro photothermal conversion ability; (**C** and **D**) in vivo photothermal conversion ability in the gel; (**E**) photothermal conversion stability; (**F**) in vivo retention of the hybrid hydrogels; (**G**) B16F10 cell viability after different treatments with or without laser; (**H**) live/dead images of B16F10 cells after different treatments; bar: 100 μm.

https://doi.org/10.2147/IJN.S409674 DovePress

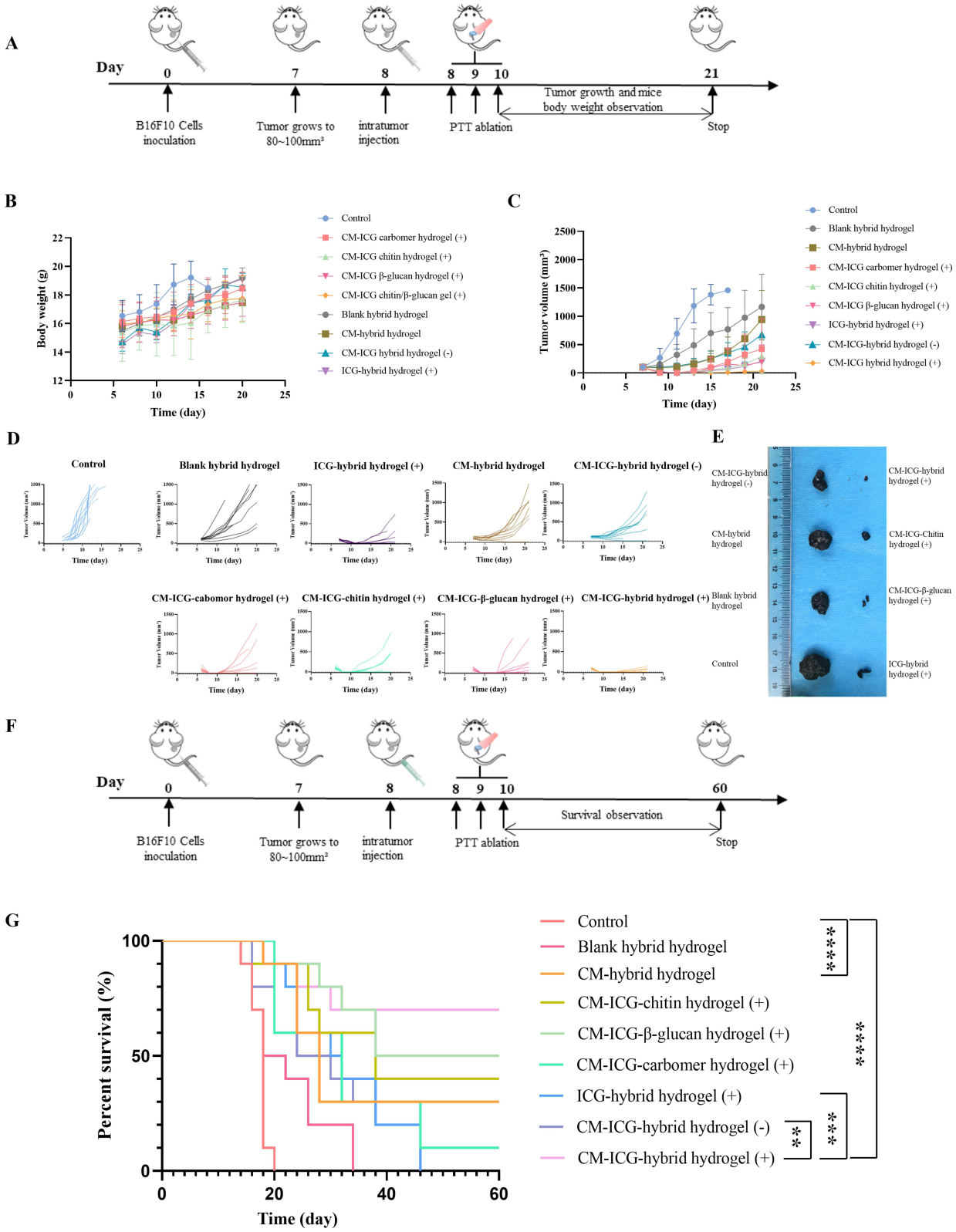

Figure 3 The inhibitory effect of different treatment groups on the primary tumor in the melanoma mouse model. (**A**) Time line; (**B**) the weight records of mice under different treatments; (**C**) the average volume size of the melanoma under different treatments; (**D**) the volume records of the primary melanoma in each group. (**E**) Flow chart of the 60-day survival test; (**F**) time line; (**G**) 60-day survival rate of mice under different treatments (Log-rank (Mantel–Cox) test, ** denotes P <0.01, *** denotes P <0.001, **** denotes P <0.0001).

ICG hybrid hydrogel (+) was abruptly interrupted by laser irradiation, and the growth of tumor in the later stage was significantly slower, indicating that PTT could rapidly ablate the tumor and exhibit a synergistic effect with immunotherapy. Although the tumor growth rates in CM-ICG-hybrid hydrogel (+) group, CM-ICG-Chitin hydrogel (+) group, and CM-ICG -β-glucan hydrogel group (+) were basically the same in the early stage (after laser irradiation), the tumor growth rate of the CM-ICG-hybrid hydrogel (+) group was significantly slower in the late stage. This may be due to the stronger immune activation effect of hybrid hydrogel.

The 60-Day Survival Test

A 60-day survival test was also undertaken (Figure 3E) after in-situ treatment of mice, and the result is shown in Figure 3F. All the mice died in 20 days in the control group, while for the blank hybrid hydrogel group all the mice died in 34 days. The mice in ICG-hybrid hydrogen (+) group and CM-ICG hybrid hydrogel (-) group were all dead in 46 days. CM-ICG-hybrid hydrogel (+) significantly improved the 60-day survival rate of mice to 70% (Figure 3G), which was significantly higher than that of other groups. Therefore, CM-ICG-hybrid hydrogel (+) exhibited the best anti-melanoma effect. Also, H&E staining was performed on main organs of surviving mice at the end of experiment, no significant metastasis was observed (Figure S3).

Pathological Analysis of the Melanoma

The pathological changes in the melanoma caused by different treatments were analyzed after H+E staining. The melanoma in the control group grew well, the cell arrangement was uniform and compact, the nuclear morphology was intact, and no obvious damage was observed (Figure 4A). In the blank hybrid hydrogel group, tissue damage and bleeding were observed. In the CM-hybrid hydrogel group, tissue damage, bleeding, nuclear pyknosis, and nucleolysis were observed, which usually appeared in apoptotic or necrotic cells.[53] ICG-hybrid hydrogel (+) could also significantly induce melanoma tissue damage. In the CM-ICG-hybrid hydrogel (+) group, nuclear damage, sparser cell arrangement, large areas of bleeding, and necrosis were observed, which indicated the strongest melanoma-killing and inhibition effect of CM-ICG-hybrid hydrogel (+).

Melanoma Cell Proliferation and Apoptosis Analysis

A large area of ki-67 positive cells and a small number of apoptotic cells were observed in the control group (Figure 4B–D), while the proportion of ki-67 positive cells (which were stained brown) decreased and the proportion of apoptotic cells increased in all treatment groups. Compared with the blank hybrid hydrogel group, the proliferation of melanoma cells in CM-hybrid hydrogel and ICG-hybrid hydrogel (+) groups was significantly decreased, and the apoptosis was significantly increased, indicating that the efficacy of blank hybrid hydrogel was optimized by PTT or the encapsulation of CM. In the CM-ICG-hybrid hydrogel (+) group, the proportion of ki-67 positive cells and non-apoptotic cells was the lowest, implying that the combination of immunotherapy and PTT could nearly completely stop the proliferation of melanoma cells and promote its apoptosis.

Immune Activation Effect

The immunoregulatory effects of different treatments were evaluated according to the procedures illustrated in Figure 5A. The levels of TNF-α and IFN-γ in all treatment groups were significantly higher than in the control group (Figure 5B and C). Among all the treatment groups, the levels of TNF-α and IFN-γ in the in CM-ICG-hybrid hydrogel (+) group were the highest. Spleen is the place where mature lymphocytes reside and directly participate in a variety of immune responses.[54,55] The proportion and differentiation of T cells in the spleen in different groups were analyzed by flow cytometry. As shown in Figure 5D and E, the percentages of T cells in the CM-hybrid hydrogel group and the ICG-hybrid hydrogel (+) group were 22.8±1.19% and 23.9±3.36%, respectively, which were significantly higher than that of the control group (12.57±0.93%). Therefore, CM-hybrid hydrogel and photothermal therapy could effectively promote the proliferation of spleen T cells. It is worth noting that the percentage of T cells in spleen of the CM-ICG-hybrid hydrogel (+) group was 36.13±2.26%, which was the highest, indicating that PTT and immunotherapy could synergistically activate the proliferation of T cells in spleen.

Effector T cells are immune cells that play an important role in anti-tumor immune response.[56,57] After being stimulated by antigen, initial T cells proliferate and differentiate into effector T cells and memory T cells.[57,58] Effector T cells include helper T cells, regulatory T cells, and killer T cells.[56,58,59] Killer T cells can directly kill antigen-carrying cells. Helper T cells secrete cytokines that can inhibit or activate other immune cells, and directly kill tumor cells by secreting granzyme.[56,60] Therefore,

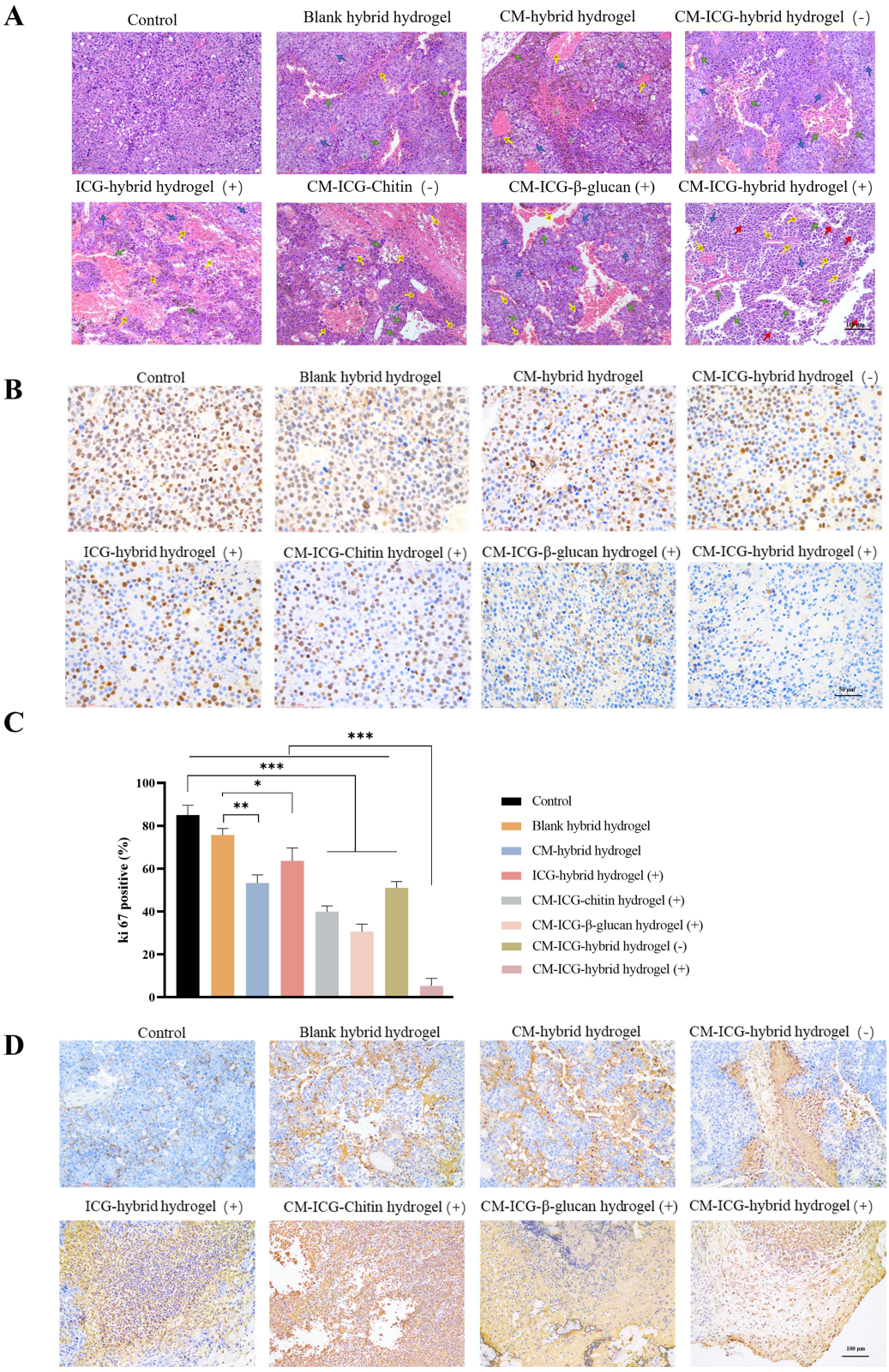

Figure 4 The pathological changes in the primary melanoma after different treatments. (**A**) H+E staining of the melanoma (green: tissue necrosis; yellow: bleeding; gray: inflammatory infiltration; blue: pycnosis and nucleolysis; red: sparsely arranged cells); (**B** and **C**) ki-67 immunohistochemical staining of the melanoma sections; (**D**) TUNEL immunohistochemical staining of the melanoma sections. **P*<0.05, ***P*<0.01, ****P*<0.001.

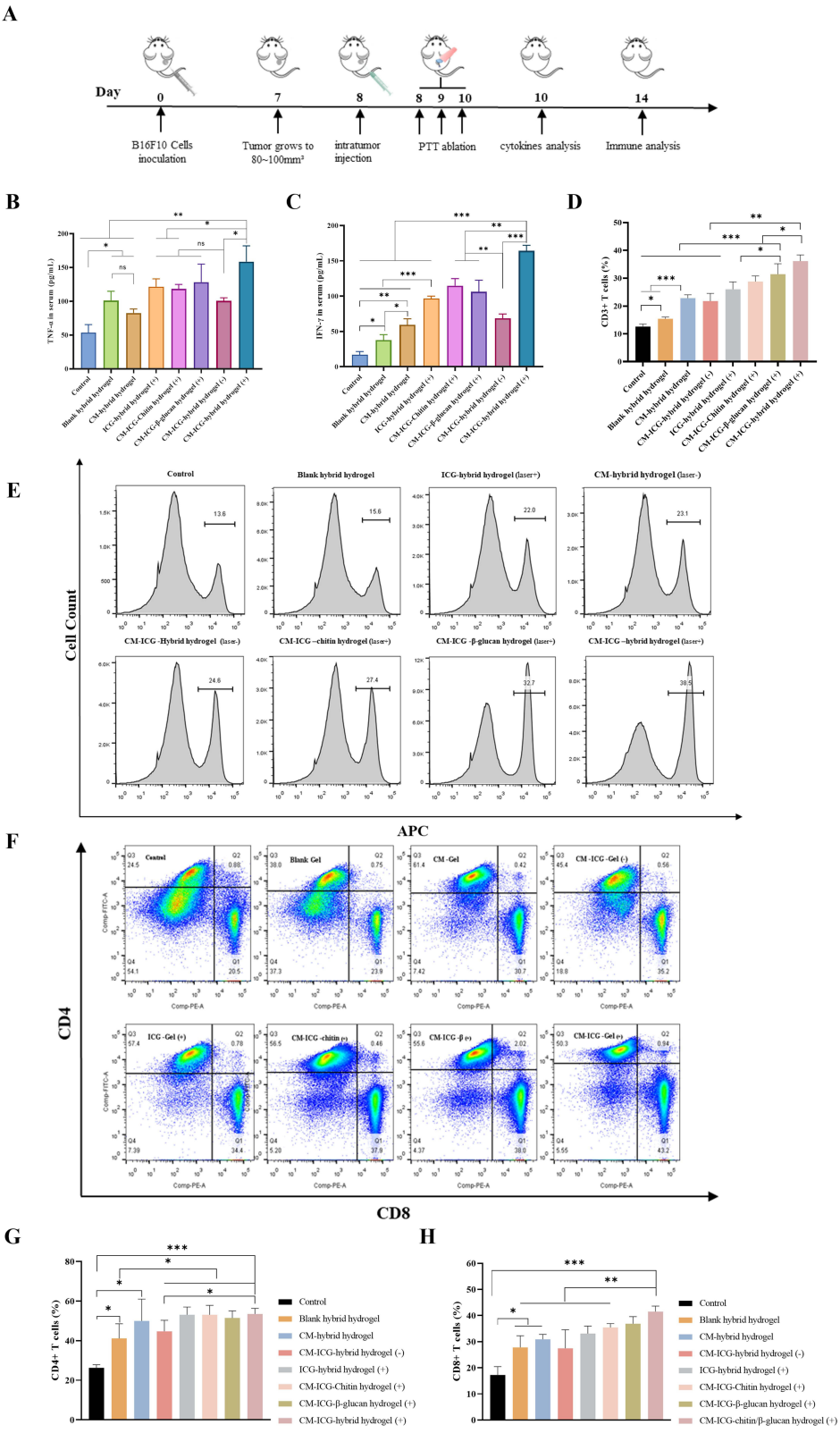

Figure 5 The immunoregulatory effects of different treatments. (**A**) Time line; (**B**) ELISA analysis of the TNF-α level in serum; (**C**) ELISA analysis of the IFN-γ level in serum; (**D**) quantitation of T cells in the spleen analyzed by flow cytometry; (**E**) flow cytometry analysis of the proportion of T cells in the spleen; (**F**) the proportion of effector T cells ($CD3^+$ $CD8^+$ T cells) and helper T cells ($CD3^+$ $CD4^+$ T cells) in the spleen; (**G**) quantitation of helper T cells analyzed by flow cytometry; (**H**) quantitation of effector T cells analyzed by flow cytometry. **P*<0.05, ***P*<0.01, ****P*<0.001.

under the gating strategy as shown in Figure S4, the proportion of helper T cells ($CD3^+$ $CD4^+$ T cells) and effector killer T cells ($CD3^+$ $CD8^+$ T cells) in the spleen were further analyzed. As shown in Figure 5F–H, in the control group, the proportion of helper T cells was only 26.27±1.57% and that of killer T cells was merely 17.26±2.31%. While, for the blank hybrid hydrogel group, the CM-hybrid hydrogel group, and the CM-ICG-hybrid hydrogel (+) group, the proportions of helper T cells were significantly increased to 41.14±7.462%, 50.00±11.07%, and 53.51±2.79%, respectively, the killer T cells increased to 27.80±4.8%, 30.9 ±1.91%, and 41.53±2.08%, respectively. Therefore, the combination of PTT and immunotherapy could significantly increase the proportion of helper T cells and effector T cells in spleen. This result was correlated well with the melanoma growth, the survival of melanoma-bearing mice, and pathological analyses.

In conclusion, CM-ICG-hybrid hydrogel (+) rapidly ablated the primary melanoma, promoted the proliferation and differentiation of T cells, activated T cell related immune response, inhibited melanoma cell proliferation, promoted melanoma apoptosis, and improved the survival of mice after treatment.

Melanoma-Preventing Effect of the CM-ICG-Hybrid Hydrogel

Distal Melanoma Growth Monitor

A distal secondary melanoma model in mice was used to investigate the preventive effect of CM-ICG-hybrid hydrogel on melanoma recurrence, and the specific procedures are illustrated in Figure 6A. The growth of secondary tumors in all

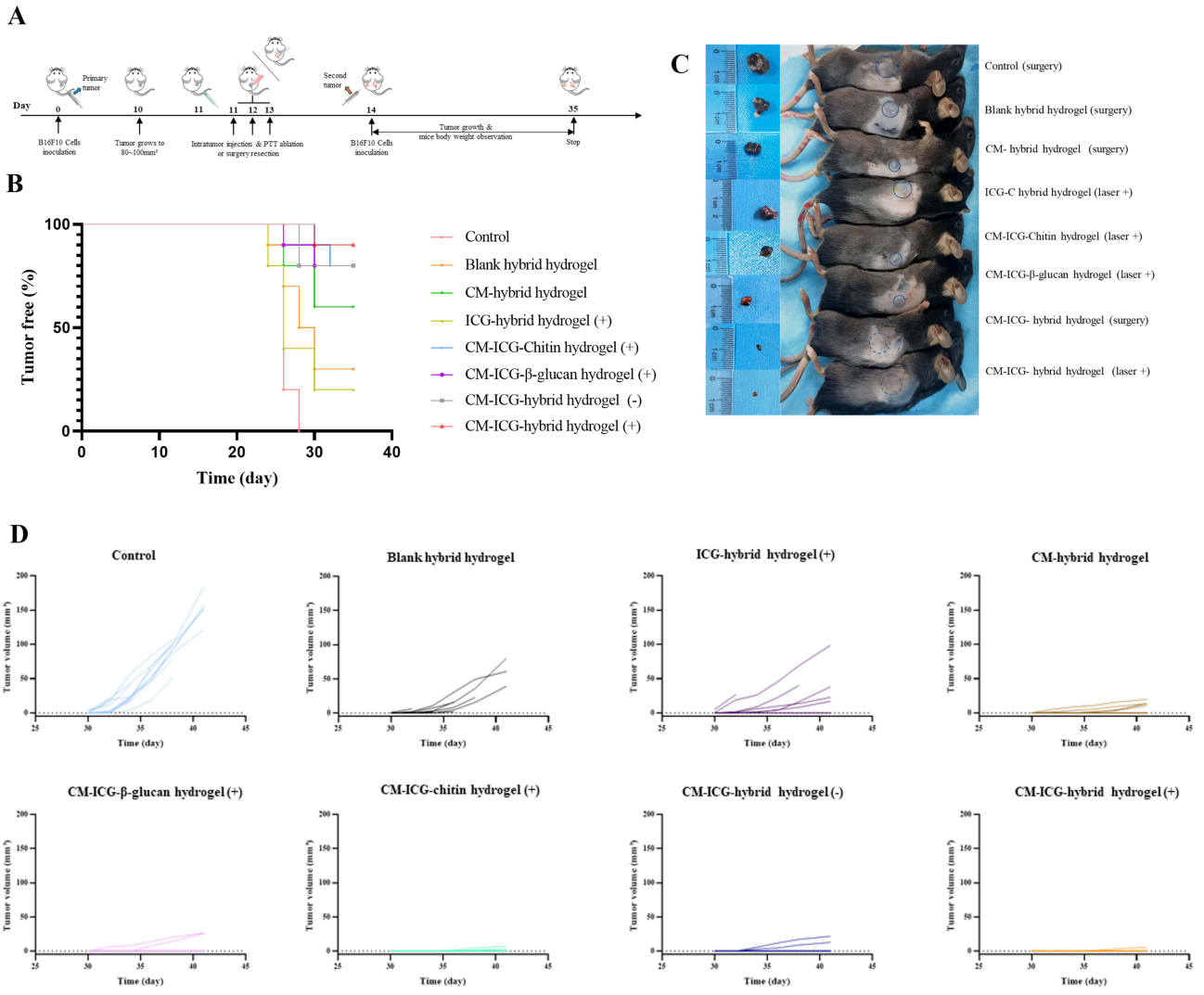

Figure 6 The inhibitory effect of different treatments on distal secondary melanoma in mice. (**A**) Time line; (**B**) the occurrence and development of secondary melanoma in mice; (**C**) images of the distal secondary melanoma; (**D**) the volume records of the distal second melanoma in each group.

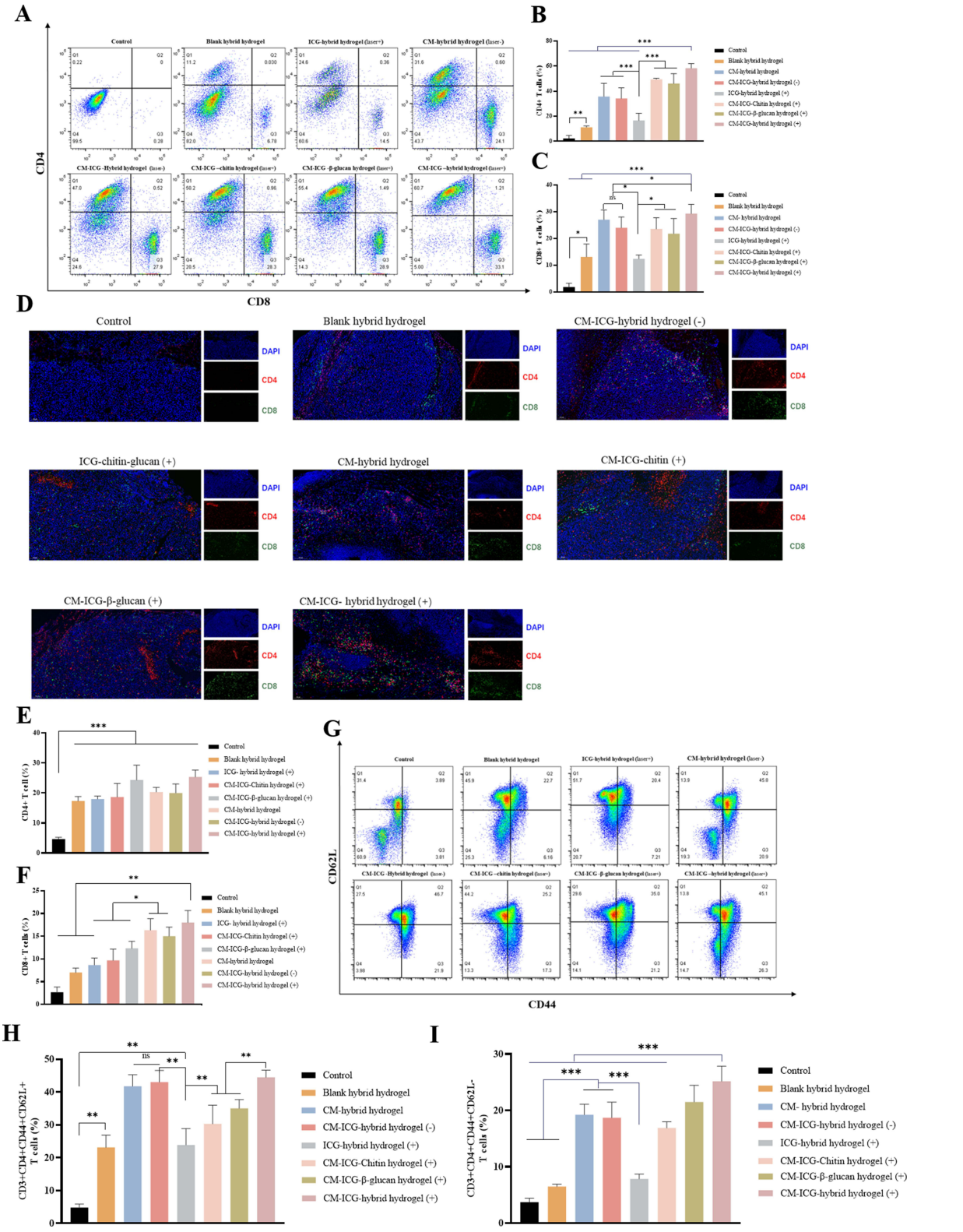

Figure 7 The immunoregulatory effects of different treatments on the distal secondary melanoma. (**A**) The activation tumor infiltrating T cells in secondary melanoma; (**B**) the proportion of helper T cells in tumor infiltrating T cells in the secondary melanoma; (**C**) the proportion of cytotoxic T cells in tumor infiltrating T cells in the secondary melanoma; (**D**) immune status of the distal secondary melanoma; (**E**) the helper T cells in the secondary melanoma sections after immunofluorescent staining; (**F**) the cytotoxic T cells in the secondary melanoma sections after immunofluorescent staining; (**G**) the detection of central memory T cells and effector memory T cells in the spleen via flow cytometry; (**H**) the proportion of central memory T cells in the spleen; (**I**) the proportion of effector memory T cells in the spleen. **P*<0.05, ***P*<0.01, ****P*<0.001.

treatment groups was significantly sluggish, and the 60-day survival rate was significantly improved compared with the control group (Figure 6B–D). In the blank hybrid hydrogel and the ICG-hybrid hydrogel (+) groups, 70% and 80% of mice developed secondary tumors within 14 days after inoculation, indicating their limited preventing effect. The incidence of secondary tumors in mice in the CM-containing groups was less than 40%, and it was only 10% in the CM-ICG-hybrid hydrogel (+) group, which was the lowest, indicating that CM and PTT together induced a stronger immune memory effect.

T-Cell Infiltration in Distal Second Tumors

The proportions of effector killer T cells and helper T cells in the secondary tumors of different groups were detected by flow cytometry. As shown in Figure 7A–C, the levels of $CD3^+$ $CD4^+$ T cells and $CD3^+$ $CD8^+$ T cells in the distal secondary tumors of the control group were very low, about 2.23±2.34% and 1.78±1.46%, indicating that the removal of primary tumors by surgery could not activate the specific immune response. However, the proportions of $CD3^+$ $CD4^+$ T cells and $CD3^+$ $CD8^+$ T cells in the ICG-hybrid hydrogel (+) group were about 16.59±5.71% and 13.37±0.2.23%, which were also significantly higher than those in the control group. This may be due to the release of a large number of tumor-associated antigens by thermal ablation in the treatment of primary tumors with PTT.[13,15,50] The released antigen could also activate the memory T cells to a certain extent, thereby generating a strong immune response when the secondary tumor attacked.[53,57] In the CM-ICG-hybrid hydrogel (+) group, the proportions of $CD3^+$ $CD4^+$ T cells and $CD3^+$ $CD8^+$ T cells were the highest, about 56.00 ±7.71% and 28.9±33.90%, indicating that CM, hybrid hydrogel, and photothermal effects synergistically induced the strongest immune activation effect. Similarly, as shown in Figure 7D, there were almost no $CD4^+$ T cells or $CD8^+$ T cells in the secondary tumor in the control group, indicating a lack of immune activation. The numbers of $CD4^+$ T cells and $CD8^+$ T cells in secondary tumors in CM-ICG-hybrid hydrogel (+) groups were the highest (Figure 7E and F).

The proportions of central memory T cells ($CD3^+$ $CD8^+$ $CD44^+$ $CD62L^+$) and effector memory T cells ($CD3^+$ $CD8^+$ $CD44^+$ $CD62L^-$) in the distal secondary tumors of different groups were also detected by flow cytometry. As shown in Figure 7H and I, the percentage of central memory T cells in spleens of control mice was only 4.827±1.03%, and the content of effector memory T cells was only 3.72±0.689% (Figure 7G – I). The proportion of central memory T cells was significantly increased to 23.133±3.769% and 23.900±4.979% in the blank hybrid hydrogel and the ICG-hybrid hydrogel (+) groups, and the content of effector memory T cells increased to 6.473±0.451% and 7.843±0.866%, respectively. Therefore, the hybrid hydrogel and PTT could induce a higher proportion of central memory T cells and effector memory T cells. In the CM-ICG-hybrid hydrogel (+) group, the proportions of central memory T cells and effector memory T cells were increased significantly to 44.5±2.163% and 25.167±2.686%, respectively, implying that CM, hybrid hydrogel, and PTT synergistically induced the largest number of memory T cells in mice. The results were consistent with the proportions of effector T cells and helper T cells in the distal secondary tumors of each group.

In conclusion, in the CM-ICG-hybrid hydrogel (+) group, a synergistic anti-melanoma effect among PTT, CM, and hybrid hydrogel were observed. It could effectively stimulate the proliferation and activation of T cells and memory T cells to achieve a long-term anti-tumor immune response and better anti-melanoma effects.

Conclusions

In this study, a novel injectable ICG-CM hybrid hydrogel was prepared, which could achieve a long-lasting combination effect of PTT and immunotherapy to treat and prevent melanoma. It quickly ablated the primary melanoma, effectively inhibited its growth, and promoted the proliferation and activation of T cells. It also activated the memory T cells, producing a long-term immune memory effect to efficiently inhibit tumor metastasis and recurrence. Our study has provided a foundation for future clinical application of the patients' tumor membrane loaded hybrid hydrogel.

Acknowledgments

We are grateful for the financial support from the Natural Science Foundation of Shaanxi Province (grant numbers 2021SF-118) and National Natural Science Foundation of China (grant numbers 81973409, 82204631).

Disclosure

The authors declare that they have no known competing interests or personal relationships that could have appeared to influence the work reported in this paper.

References

1. Garbe C, Eigentler TK, Keilholz U, Hauschild A, Kirkwood JM. Systematic review of medical treatment in melanoma: current status and future prospects. *Oncologist*. 2011;16(1):5–24. doi:10.1634/theoncologist.2010-0190
2. Li C, Chi S, Xie J. Hedgehog signaling in skin cancers. *Cell Signal*. 2011;23(8):1235–1243. doi:10.1016/j.cellsig.2011.03.002
3. Mattia G, Puglisi R, Ascione B, Malorni W, Carè A, Matarrese P. Cell death-based treatments of melanoma: conventional treatments and new therapeutic strategies. *Cell Death Dis*. 2018;9(2):112. doi:10.1038/s41419-017-0059-7
4. Garbe C, Peris K, Hauschild A, et al. Diagnosis and treatment of melanoma: European consensus-based interdisciplinary guideline. *Eur J Cancer*. 2010;46(2):270–283. doi:10.1016/j.ejca.2009.10.032
5. Harries M, Malvehy J, Lebbe C, et al. Treatment patterns of advanced malignant melanoma (stage III–IV) – a review of current standards in Europe. *Eur J Cancer*. 2016;60:179–189. doi:10.1016/j.ejca.2016.01.011
6. Bhatia S, Tykodi SS, Thompson JA. Treatment of metastatic melanoma: an overview. *Oncology*. 2009;23(6):488–496.
7. Payandeh Z, Yarahmadi M, Nariman-Saleh-Fam Z, et al. Immune therapy of melanoma: overview of therapeutic vaccines. *J Cell Physiol*. 2019;234:14612–14621. doi:10.1002/jcp.28181
8. Butnariu M, Quispe C, Herrera-Bravo J, et al. The effects of thymoquinone on pancreatic cancer: evidence from preclinical studies. *Biomed Pharmacother*. 2022;153:113364. doi:10.1016/j.biopha.2022.113364
9. Butnariu M, Quispe C, Herrera-Bravo J, et al. Papaver plants: current insights on phytochemical and nutritional composition along with biotechnological applications. *Oxid Med Cell Longev*. 2022;2022:2041769. doi:10.1155/2022/2041769
10. Shao J, Xie H, Huang H, et al. Biodegradable black phosphorus-based nanospheres for in vivo photothermal cancer therapy. *Nat Commun*. 2016;7(1):12967. doi:10.1038/ncomms12967
11. Heidari M, Sattarahmady N, Azarpira N, Heli H, Mehdizadeh AR, Zare T. Photothermal cancer therapy by gold-ferrite nanocomposite and near-infrared laser in animal model. *Lasers Med Sci*. 2016;31(2):221–227. doi:10.1007/s10103-015-1847-x
12. Shirata C, Kaneko J, Inagaki Y, et al. Near-infrared photothermal/photodynamic therapy with indocyanine green induces apoptosis of hepatocellular carcinoma cells through oxidative stress. *Sci Rep*. 2017;7(1):13958. doi:10.1038/s41598-017-14401-0
13. Chen Q, Xu L, Liang C, Wang C, Peng R, Liu Z. Photothermal therapy with immune-adjuvant nanoparticles together with checkpoint blockade for effective cancer immunotherapy. *Nat Commun*. 2016;7(1):13193. doi:10.1038/ncomms13193
14. Yoon H-J, Lee H-S, Lim J-Y, Park J-H. Liposomal indocyanine green for enhanced photothermal therapy. *ACS Appl Mater Interfaces*. 2017;9(7):5683–5691. doi:10.1021/acsami.6b16801
15. Nam J, Son S, Ochyl LJ, Kuai R, Schwendeman A, Moon JJ. Chemo-photothermal therapy combination elicits anti-tumor immunity against advanced metastatic cancer. *Nat Commun*. 2018;9(1):1074. doi:10.1038/s41467-018-03473-9
16. Shi H, Cao T, Connolly JE, et al. Hyperthermia enhances CTL cross-priming. *J Immunol*. 2006;176(4):2134–2141. doi:10.4049/jimmunol.176.4.2134
17. Toraya-Brown S, Sheen MR, Zhang P, et al. Local hyperthermia treatment of tumors induces CD8(+) T cell-mediated resistance against distal and secondary tumors. *Nanomedicine*. 2014;10(6):1273–1285. doi:10.1016/j.nano.2014.01.011
18. Butnariu M, Quispe C, Herrera-Bravo J, et al. The pharmacological activities of crocus sativus L.: a review based on the mechanisms and therapeutic opportunities of its phytoconstituents. *Oxid Med Cell Longev*. 2022;2022:8214821. doi:10.1155/2022/8214821
19. Butnariu M, Quispe C, Herrera-Bravo J, et al. A review on Tradescantia: phytochemical constituents, biological activities and health-promoting effects. *Front Biosci*. 2022;27(6):197. doi:10.31083/j.fbl2706197
20. Luke JJ, Flaherty KT, Ribas A, Long GV. Targeted agents and immunotherapies: optimizing outcomes in melanoma. *Nat Rev Clin Oncol*. 2017;14(8):463–482. doi:10.1038/nrclinonc.2017.43
21. Knight A, Karapetyan L, Kirkwood JM. Immunotherapy in Melanoma: recent advances and future directions. *Cancers*. 2023;15(4):1106. doi:10.3390/cancers15041106
22. Butnariu M, Quispe C, Koirala N, et al. Bioactive effects of curcumin in human immunodeficiency virus infection along with the most effective isolation techniques and type of nanoformulations. *Int J Nanomedicine*. 2022;17:3619–3632. doi:10.2147/IJN.S364501
23. Li X, Naylor MF, Le H, et al. Clinical effects of in situ photoimmunotherapy on late-stage melanoma patients. *Cancer Biol Ther*. 2010;10(11):1081–1087. doi:10.4161/cbt.10.11.13434
24. Aikins ME, Xu C, Moon JJ. Engineered nanoparticles for cancer vaccination and immunotherapy. *Acc Chem Res*. 2020;53(10):2094–2105. doi:10.1021/acs.accounts.0c00456
25. Lizée G, Radvanyi LG, Overwijk WW, Hwu P. Immunosuppression in melanoma immunotherapy: potential opportunities for intervention. *Clin Cancer Res*. 2006;12(7):2359s–2365s. doi:10.1158/1078-0432.CCR-05-2537
26. Mansfield AS, Holtan SG, Grotz TE, et al. Regional immunity in melanoma: immunosuppressive changes precede nodal metastasis. *Mod Pathol*. 2011;24(4):487–494. doi:10.1038/modpathol.2010.227
27. Ramirez-Montagut T, Turk MJ, Wolchok JD, Guevara-Patino JA, Houghton AN. Immunity to melanoma: unraveling the relation of tumor immunity and autoimmunity. *Oncogene*. 2003;22(20):3180–3187. doi:10.1038/sj.onc.1206462
28. Lin MJ, Svensson-Arvelund J, Lubitz GS, et al. Cancer vaccines: the next immunotherapy frontier. *Nat Cancer*. 2022;3(8):911–926. doi:10.1038/s43018-022-00418-6
29. Shao K, Singha S, Clemente-Casares X, Tsai S, Yang Y, Santamaria P. Nanoparticle-based immunotherapy for cancer. *ACS Nano*. 2015;9(1):16–30. doi:10.1021/nn5062029
30. Leleux J, Roy K. Micro and nanoparticle-based delivery systems for vaccine immunotherapy: an immunological and materials perspective. *Adv Healthcare Mater*. 2013;2(1):72–94. doi:10.1002/adhm.201200268
31. Wilson JT, Keller S, Manganiello MJ, et al. pH-responsive nanoparticle vaccines for dual-delivery of antigens and immunostimulatory oligonucleotides. *ACS Nano*. 2013;7(5):3912–3925. doi:10.1021/nn305466z

32. Kang XM, Lei JX, Yang C, et al. A hybrid hydrogel composed of chitin and beta-glucan for the effective management of wound healing and scarring. *Biomater Sci*. 2022;10(20):6024–6036.
33. Chan GC, Chan WK, Sze DM. The effects of beta-glucan on human immune and cancer cells. *J Hematol Oncol*. 2009;2:25. doi:10.1186/1756-8722-2-25
34. Elieh Ali Komi D, Sharma L, Dela Cruz CS. Chitin and its effects on inflammatory and immune responses. *Clin Rev Allergy Immunol*. 2018;54 (2):213–223. doi:10.1007/s12016-017-8600-0
35. Jiang X, Bao H, Merzendorfer H, Yang Q. Immune responses of mammals and plants to chitin-containing pathogens. *Adv Exp Med Biol*. 2019;1142:61–81.
36. Xu X, Yasuda M, Nakamura-Tsuruta S, Mizuno M, Ashida H. β-glucan from lentinus edodes inhibits nitric oxide and tumor necrosis factor-α production and phosphorylation of mitogen-activated protein kinases in lipopolysaccharide-stimulated murine RAW 264.7 macrophages*. *J Biol Chem*. 2012;287(2):871–878. doi:10.1074/jbc.M111.297887
37. De Marco Castro E, Calder PC, Roche HM. β-1,3/1,6-glucans and immunity: state of the art and future directions. *Mol Nutr Food Res*. 2021;65(1): e1901071. doi:10.1002/mnfr.201901071
38. Albeituni SH, Yan J. The effects of β-glucans on dendritic cells and implications for cancer therapy. *Anticancer Agents Med Chem*. 2013;13 (5):689–698. doi:10.2174/1871520611313050003
39. Yang R, Xu J, Xu L, et al. Cancer cell membrane-coated adjuvant nanoparticles with mannose modification for effective anticancer vaccination. *ACS Nano*. 2018;12(6):5121–5129. doi:10.1021/acsnano.7b09041
40. Li R, He Y, Zhang S, Qin J, Wang J. Cell membrane-based nanoparticles: a new biomimetic platform for tumor diagnosis and treatment. *Acta Pharm Sin B*. 2018;8(1):14–22. doi:10.1016/j.apsb.2017.11.009
41. Kang X, Lei J, Yang C, et al. A hybrid hydrogel composed of chitin and β-glucan for the effective management of wound healing and scarring. *Biomater Sci*. 2022;10(20):6024–6036. doi:10.1039/D2BM00935H
42. Chen Q, Huang G, Wu W, et al. A hybrid eukaryotic-prokaryotic nanoplatform with photothermal modality for enhanced antitumor vaccination. *Adv Mater*. 2020;32(16):e1908185. doi:10.1002/adma.201908185
43. Fang RH, Hu CM, Luk BT, et al. Cancer cell membrane-coated nanoparticles for anticancer vaccination and drug delivery. *Nano Lett*. 2014;14 (4):2181–2188. doi:10.1021/nl500618u
44. Ossio R, Roldán-Marín R, Martínez-Said H, Adams DJ, Robles-Espinoza CD. Melanoma: a global perspective. *Nat Rev Cancer*. 2017;17 (7):393–394. doi:10.1038/nrc.2017.43
45. Ahmed EM. Hydrogel: preparation, characterization, and applications: a review. *J Adv Res*. 2015;6(2):105–121. doi:10.1016/j.jare.2013.07.006
46. Schoenmakers DC, Rowan AE, Kouwer PHJ. Crosslinking of fibrous hydrogels. *Nat Commun*. 2018;9(1):2172. doi:10.1038/s41467-018-04508-x
47. Zidek J, Milchev A, Jancar J, Vilgis TA. Deformation-induced damage and recovery in model hydrogels – a molecular dynamics simulation. *J Mech Phys Solids*. 2016;94:372–387. doi:10.1016/j.jmps.2016.05.013
48. Jeon O, Song SJ, Lee K-J, et al. Mechanical properties and degradation behaviors of hyaluronic acid hydrogels cross-linked at various cross-linking densities. *Carbohydr Polym*. 2007;70(3):251–257. doi:10.1016/j.carbpol.2007.04.002
49. Taylor DL, in het Panhuis M. Self-Healing Hydrogels. *Adv Mater*. 2016;28(41):9060–9093. doi:10.1002/adma.201601613
50. Ma Y, Zhang Y, Li X, et al. Near-infrared II phototherapy induces deep tissue immunogenic cell death and potentiates cancer immunotherapy. *ACS Nano*. 2019;13(10):11967–11980. doi:10.1021/acsnano.9b06040
51. Ni JS, Zhang X, Yang G, et al. A photoinduced nonadiabatic decay-guided molecular motor triggers effective photothermal conversion for cancer therapy. *Angew Chem Int Ed Engl*. 2020;59(28):11298–11302. doi:10.1002/anie.202002516
52. Rao L, G-t Y, Meng Q-F, et al. Cancer cell membrane-coated nanoparticles for personalized therapy in patient-derived xenograft models. *Adv Funct Mater*. 2019;29(51):1905671. doi:10.1002/adfm.201905671
53. Luo L, Zhu C, Yin H, et al. Laser immunotherapy in combination with perdurable PD-1 blocking for the treatment of metastatic tumors. *ACS Nano*. 2018;12(8):7647–7662. doi:10.1021/acsnano.8b00204
54. Lewis SM, Williams A, Eisenbarth SC. Structure and function of the immune system in the spleen. *Sci Immunol*. 2019;4(33). doi:10.1126/sciimmunol.aau6085
55. Mebius RE, Kraal G. Structure and function of the spleen. *Nat Rev Immunol*. 2005;5(8):606–616.
56. Yang Y. Cancer immunotherapy: harnessing the immune system to battle cancer. *J Clin Invest*. 2015;125(9):3335–3337. doi:10.1172/JCI83871
57. Thakur A, Kondadasula SV, Ji K, et al. Anti-tumor and immune modulating activity of T cell induced tumor-targeting effectors (TITE). *Cancer Immunol Immunother*. 2021;70(3):633–656. doi:10.1007/s00262-020-02692-8
58. Kaech SM, Wherry EJ, Ahmed R. Effector and memory T-cell differentiation: implications for vaccine development. *Nat Rev Immunol*. 2002;2 (4):251–262. doi:10.1038/nri778
59. Kennedy R, Celis E. Multiple roles for CD4+ T cells in anti-tumor immune responses. *Immunol Rev*. 2008;222:129–144. doi:10.1111/j.1600-065X.2008.00616.x
60. Salti SM, Hammelev EM, Grewal JL, et al. Granzyme B regulates antiviral CD8+ T cell responses. *J Immunol*. 2011;187(12):6301–6309. doi:10.4049/jimmunol.1100891